"Ideal" tearing and the transition to fast reconnection in the weakly collisional MHD and EMHD regimes

Daniele del Sarto, Fulvia Pucci, Anna Tenerani, Marco Velli

AGU PUBLICATIONS

JGR

Journal of Geophysical Research: Space Physics

RESEARCH ARTICLE
10.1002/2015JA021975

Key Points:
- The critical scalings of the ideal tearing are generalized in the inertia-driven regime
- FLR effects reduce the critical aspect ratio for the transition to the ideal tearing
- The ideal tearing model may explain a nonlinear reconnection rate increase of primary tearing modes

Correspondence to:
D. Del Sarto,
daniele.del-sarto@univ-lorraine.fr

Citation:
Del Sarto, D., F. Pucci, A. Tenerani, and M. Velli (2016), "Ideal" tearing and the transition to fast reconnection in the weakly collisional MHD and EMHD regimes, *J. Geophys. Res. Space Physics*, *121*, 1857–1873, doi:10.1002/2015JA021975.

Received 1 OCT 2015
Accepted 24 FEB 2016
Accepted article online 27 FEB 2016
Published online 25 MAR 2016

"Ideal" tearing and the transition to fast reconnection in the weakly collisional MHD and EMHD regimes

Daniele Del Sarto[1], Fulvia Pucci[2], Anna Tenerani[3], and Marco Velli[3]

[1]Institut Jean Lamour, Université de Lorraine, Nancy, France, [2]Dipartimento di Fisica, Università degli Studi di Roma Tor Vergata, Rome, Italy, [3]Earth, Planetary and Space Sciences, University of California, Los Angeles, California, USA

Abstract This paper discusses the transition to fast growth of the tearing instability in thin current sheets in the collisionless limit where electron inertia drives the reconnection process. It has been previously suggested that in resistive MHD there is a natural maximum aspect ratio (ratio of sheet length and breadth to thickness) which may be reached for current sheets with a macroscopic length L, the limit being provided by the fact that the tearing mode growth time becomes of the same order as the Alfvén time calculated on the macroscopic scale. For current sheets with a smaller aspect ratio than critical the normalized growth rate tends to zero with increasing Lundquist number S, while for current sheets with an aspect ratio greater than critical the growth rate diverges with S. Here we carry out a similar analysis but with electron inertia as the term violating magnetic flux conservation: previously found scalings of critical current sheet aspect ratios with the Lundquist number are generalized to include the dependence on the ratio d_e^2/L^2, where d_e is the electron skin depth, and it is shown that there are limiting scalings which, as in the resistive case, result in reconnecting modes growing on ideal time scales. Finite Larmor radius effects are then included, and the rescaling argument at the basis of "ideal" reconnection is proposed to explain secondary fast reconnection regimes naturally appearing in numerical simulations of current sheet evolution.

1. Introduction

Magnetic reconnection is thought to be the mechanism underlying many explosive phenomena observed in both space and laboratory plasmas, ranging from magnetospheric substorms, to solar flares and coronal mass ejections, to the sawtooth crashes observed in tokamaks. The classic picture of reconnection involves current sheets, most often assumed to be planar like and concentrated more narrowly in the third dimension. Often, a guide magnetic field lies within the current sheet itself, so that the actual three-dimensional field does not vanish in the sheet. Different models for reconnection occurring in such quasi 2-D configurations have been developed, two prominent, different examples being the Sweet-Parker (SP) stationary reconnection scenario and the spontaneous reconnecting modes naturally developing due to the tearing instability of the current sheet itself. *Biskamp* [1986] first pointed out the important role played by the current sheet aspect ratio in determining whether a stationary reconnection configuration could be reached. He found, via numerical simulations, that the SP current sheet could become unstable to reconnecting modes once a critical value of the Lundquist number (estimated on the current sheet length or breadth, L) of about $S \simeq 10^4$ was exceeded. A detailed examination of the stability of the SP configuration led to the definition of the plasmoid chain instability [*Loureiro et al.*, 2007], reminiscent of the plasmoid-induced reconnection concept and fractal reconnection models introduced by *Shibata and Tanuma* [2001]. Recently, *Pucci and Velli* [2014] have pointed out that the divergence of the growth rate of the plasmoid chain instability in the limit of large Lundquist number within resistive MHD implies that current sheets should never elongate sufficiently to achieve the SP aspect ratio. They have shown that a critical aspect ratio separates slowly unstable current sheets (with growth rate scaling as a negative, fractional exponent of the Lundquist number) from violently unstable ones (growth rates scaling with a positive power of S). They dubbed the instability of the critically unstable current sheet "ideal tearing" (hereafter IT), because the growth rate, normalized to the Alfvén time *along the sheet* L, becomes of order unity and independent of the Lundquist number itself.

The large predicted growth rates and the presence of critical values for dimensionless numbers such as current sheet aspect ratio make the described instabilities good candidates to understand and model the mechanisms behind observed fast reconnection phenomena [*Velli et al.*, 2015]. Indeed, to date there is no agreed

theoretical explanation for the fast time scales over which reconnection events develop in nature nor for their triggering, while evidence from both experiments and numerical simulations points to the importance of small-scale formation and kinetic effects, [*Daughton et al.*, 2011; *Moser and Bellan*, 2012; *Biancalani and Scott*, 2012] which are theoretically expected to lead to Alfvénic (or "ideal") reconnection in 3-D configurations as well [*Boozer*, 2012]. Moreover, numerical simulations of tearing mode instabilities have identified a secondary, nonlinear, increase of the reconnection rate that has been sometimes interpreted in terms of a nascent plasmoid-unstable SP regime [*Loureiro et al.*, 2005; *Ali et al.*, 2014] or generically a secondary "explosive reconnection" regime [*Biancalani and Scott*, 2012]. A nonlinear increase of the reconnection rate on ideal, Alfvénic time scales was also numerically measured by *Yu et al.* [2014] in simulations of low mode number reconnection instabilities. Given the recent developments of the theory of large aspect ratio current sheet instabilities, it is important to understand whether such augmented fast reconnection rates may indeed be interpreted as fast secondary instabilities of the nonlinearly generated current sheets stemming from the primary reconnection event. Specifically, given that kinetic and two-fluid effects easily become dominant compared to classical, collisional resistivity at small spatial scales, it seems timely to see whether and how such effects modify the transition to an IT regime.

The present paper focuses on the extension of the IT scaling arguments to weakly collisional regimes where reconnection is mediated by electron inertia effects and on whether such generalized IT regimes might explain the nonlinear occurrence of fast exponentially growing reconnection rates. We will consider both the incompressible reduced MHD (RMHD) [see, e.g., *Zank and Matthaeus*, 1992] and electron MHD (EMHD) [*Kingsep et al.*, 1990] frequency ranges, where the perturbations are dominated by Alfvén and whistler modes, respectively. The formal similarity between RMHD and EMHD reconnection in slab geometry, previously discussed in [*Del Sarto et al.*, 2003, 2006], allows a unified treatment for the onset of IT in an electron inertia-driven framework.

Within a fluid modeling, electron inertia has long been considered the most promising alternative to standard resistive reconnection thanks to its greater weight with respect to resistivity in the generalized Ohm's law of quasi-collisionless plasmas [*Coppi*, 1964a, 1964b; *Wesson*, 1990; *Porcelli*, 1991]. Astrophysical and thermonuclear fusion plasmas are examples of such systems, since their particle mean-free path typically exceeds the characteristic hydrodynamic lengths by order(s) of magnitude. In general, interspecies collisions may be neglected with respect to inertial terms when the characteristic ion-electron collision frequency is negligible with respect to the inverse time scale of the phenomena considered [*Ottaviani and Porcelli*, 1995; *Porcelli et al.*, 2004; *Hosseinpur et al.*, 2009]. The inertial slab RMHD regime we focus on here has indeed been widely used to model basic features of magnetic reconnection in tokamak devices, for which the strong guide field approximation, of which we consider the 2-D geometry limit, was first devised. Even if this may represent a simplified assumption in many finite-β regimes of astrophysical interest [see, e.g., *Zeleney and Artemyev*, 2013], it is useful to the purpose of discussing the general validity and implications of the IT model in the fluid inertia-driven regime, taken as a first example of extension to the kinetic scales. In EMHD the neglect of collisional resistivity is even more justified, which is why EMHD reconnection is mostly studied in purely inertia-driven regimes (see *Hosseinpur et al.* [2009] for a discussion of the transition from resistive to inertial EMHD). Because of the large characteristic frequencies involved, EMHD provides a natural framework for collisionless reconnection. The relation between the convection electron flow and the magnetic field, typical of the EMHD regime, plays a prominent role in explaining the quadrupolar structure of the out-of-plane magnetic field [*Bian and Vekstein*, 2007], which is often recognized as a distinctive signature for the in situ detection of magnetospheric reconnection [*Øieroset et al.*, 2001]. *Rogers et al.* [2001] also adopted the incompressible, inertialess, collisionless EMHD model to explain the opening up of the reconnection layer in 2-D simulations with no guide field. We finally note that the present paper does not cover the framework of the so-called Hall- or whistler-mediated reconnection (Appendix A2), especially relevant to the magnetopause environment [*Birn et al.*, 2001; *Vaivads et al.*, 2014] and which is known to provide prominent examples of fast reconnection rates weakly dependent from both resistivity [*Mandt et al.*, 1994] and electron inertia [*Biskamp et al.*, 1995]. This will be considered in future works.

The paper is structured as follows. In section 2 we summarize the rescaling arguments leading to the concept of ideal tearing. In section 3 we introduce the model equations for reconnection in the RMHD and EMHD regimes and the relevant dispersion relations (section 3.1). In section 4 we extend the IT paradigm first to the inertial RMHD and EMHD reconnection regimes (section 4.1) and then to include finite Larmor radius (FLR) effects (section 4.2). We then discuss these results (section 5) by comparing the role of inertia to that

of resistivity in different natural and laboratory plasmas while commenting about the extendibility of the IT model to fully kinetic regimes (section 5.1) and by considering an application of the IT model to collisionless steady reconnecting current sheets (section 5.2). Then, we discuss how the rescaling argument might explain explosive reconnection regimes nonlinearly observed in simulations of magnetic reconnection (section 5.3) and the implications this may have on turbulent reconnection (section 5.4). Section 6 provides a summary and conclusion, and in Appendix A1 we recall the derivation of the model equations both from a two-fluid model and compared with the generalized Ohm's law (section A2).

2. The Ideal Tearing Model

Consider a current sheet of length L and thickness a. As MHD is scale free, in the classical tearing mode theory, it is customary to take the width a as normalization length, since typically, $L/a > 1$ and a is the only characteristic length defined by the (usually 1-D) equilibrium profile. However, when dealing with thin sheets with a arbitrarily small, the distinction between L and a becomes important, as the tearing mode growth rate is only small when measured with respect to the ideal Alfvén time scale based on a but can become large when measured with respect to a macroscopic scale $L >> a$ (the basic idea behind the plasmoid instability and IT is detailed below). From now on, we will label quantities normalized to the scale L with the apex "$*$", using standard notation for nondimensional quantities defined in terms of the (possibly microscopic) shear-scale a.

In this notation, the classical linear reconnecting mode on Harris-type current sheets has a maximal growth rate scaling as $\gamma_M \tau_A \sim S^{-1/2}$, where the Lundquist number $S = aV_A/\eta_m$ and $\tau_A = a/V_A$, with V_A the Alfvén speed based on the characteristic magnetic field strength far from the sheet. In the SP case, predicated on the renormalized Lundquist number $S^* = LV_A/\eta_m$, one finds immediately that $\gamma_M \tau_A^* = \gamma_M L/V_A \sim S^{*1/4}$, i.e., a growth rate which diverges with the macroscopic Lundquist number S^*. *Pucci and Velli* [2014], aiming to resolve this paradox, incompatible with the ideal MHD limit, studied large aspect ratio current sheets with L/a scaling as a positive fractional power of the Lundquist number $S^* = LV_A/\eta_m \gg 1$. They showed that when a threshold $(L/a)_{IT} \sim (S^*)^\alpha$ $(1/2 > \alpha > 0)$ is reached, the resistive tearing mode growth rate $\gamma_M \tau_A^*$ becomes of order unity and independent of S^*. This regime was named ideal tearing, in contrast to the classical tearing (hereafter CT) theory, in which the growth rates scale as a negative power of the a-normalized Lundquist number S. The large aspect ratio limit allowed *Pucci and Velli* [2014] to evaluate the characteristic CT reconnection rate through the fastest growing mode, from which the value $\alpha = 1/3$ was obtained, leading to the conclusion that SP current sheets should not form at large S^* (different equilibrium profiles may induce small deviations from this value (F. Pucci et al., to be submitted, 2016)). The renormalization in fact gives

$$\gamma_M \tau_A^* \sim (S^*)^{-1/2} (L/a)^{3/2} \tag{1}$$

and the clock whose rate defines the reconnection speed enters this renormalized theory through τ_A^* which depends itself on L, i.e., the clock set on the ideal scale L results slower by a factor a/L (or, as we shall see, $(a/L)^2$ in the EMHD regime) than the clock with which the reconnection rate is measured in the CT theory: it is thus always possible to find a critical exponent $\alpha > 0$ such that $\gamma_M \tau_A^* \simeq 1$ once the condition $(L/a) \sim (S^*)^\alpha$ is imposed. In other words, the tearing mode theory, under the assumption of a current sheet whose aspect ratio scales as a power of the (small) nonideal parameter ε^* which allows reconnection, say $(a/L)_{IT} \sim (\varepsilon^*)^\alpha$, can explain the transition to fast reconnection if the value of α is such that the growth rate of the instability is independent from ε^* itself. Notice, however, that the IT criterion may be applied in principle to any reconnection unstable aspect ratio L/a, if L is large enough with respect to a. It is, e.g., the case of tearing unstable current sheets, nonlinearly developed by primary reconnection events, which we will consider later. We now consider how this happens once electron inertia first and FLR-type effects second are taken into account.

3. Model Equations

We restrict our analysis to a 2-D system in the (x, y) plane and assume for simplicity an electron-proton plasma. Consider the incompressible equations in slab geometry. We adopt the standard "poisson bracket" representation $[f, g] \equiv \partial_x f \partial_y g - \partial_y f \partial_x g = \mathbf{e}_z \cdot (\nabla f \times \nabla g)$. The velocity stream functions φ and b are such that $\boldsymbol{U}_\perp = -\nabla\varphi \times \mathbf{e}_z$ in RMHD and $\boldsymbol{u}_\perp^e = -\nabla b \times \mathbf{e}_z$ in EMHD (see below), where "$\perp$" stands for components in the (x, y) plane and $\boldsymbol{u}^e$ and $\boldsymbol{U}$ are the electron and bulk plasma velocities, respectively. Analogously, the magnetic stream function ψ is defined through $\boldsymbol{B} = \nabla\psi(x, y) \times \mathbf{e}_z + (B_0 + b(x, y))\mathbf{e}_z$, with B_0 uniform in space. We assume an equilibrium in-plane magnetic field $\boldsymbol{B}_\perp^0 = B_y^0(x/a)\mathbf{e}_y$ with $B_y^0(x/a) = \partial_x \psi_0(x/a)$. Equilibrium quantities are

labeled with "0," and we introduce the fields $F \equiv \psi - d_e^2\nabla^2\psi$ and $W \equiv b - d_e^2\nabla^2 b$. Here $d_e \equiv c/\omega_{pe}$ is the electron skin depth.

Using a as the reference length and characteristic quantities $B_\perp^0$ and n_0 for magnetic field and densities, the model equations may then be written in nondimensional form either as

$$\frac{\partial}{\partial t}F + [\varphi, F] = \rho_s^2[\nabla^2\varphi, \psi] + S^{-1}\nabla^2\psi, \tag{2}$$

$$\frac{\partial}{\partial t}\nabla^2\varphi + [\varphi, \nabla^2\varphi] = [\psi, \nabla^2\psi] + R^{-1}\nabla^4\varphi\,, \tag{3}$$

valid in the RMHD frequency range, or

$$\frac{\partial}{\partial t}F + [b, F] = S_{\text{EMHD}}^{-1}\nabla^2\psi, \tag{4}$$

$$\frac{\partial}{\partial t}W + [b, W] = [\psi, \nabla^2\psi] + S_{\text{EMHD}}^{-1}\nabla^2 b\,, \tag{5}$$

valid in the EMHD frequency range.

In the above, time is normalized to $\tau_A \equiv (a/d_i)\Omega_i^{-1}$ in RMHD, where Ω_i is the ion cyclotron frequency and $d_i \equiv \sqrt{m_i}c/(\sqrt{m_e}\omega_{pe})$ is the ion skin depth (ω_{pe} being the usual plasma frequency and with obvious notation for the masses); in EMHD time is normalized to the inverse of the whistler frequency, $\tau_W \equiv (a/d_e)^2\Omega_e^{-1} = (a/d_i)^2\Omega_i^{-1}$. The other parameters on which the tearing reconnection rate depends are the ion sound Larmor radius, $\rho_s \equiv c_{\text{is}}/\Omega_i$ (nondimensionalized with a in equation (2)), where c_{is} is the ion sound speed, i.e., the thermal speed based on electron temperature and ion mass, $R \equiv (\nu_{\text{ii}}\tau_A)^{-1}$ (Reynold's number) with ν_{ii} the ion-ion viscosity, $S \equiv \tau_D/\tau_A$ (Alfvénic Lundquist number), and $S_{\text{EMHD}} \equiv \tau_D/\tau_W$ (EMHD Lundquist number) with $\tau_D = 4\pi a^2/(\eta c^2)$ the resistive diffusion time (η is the scalar resistivity). The physical meaning of the terms of equations (2)–(5) and their relation to both the two-fluid model equations and the generalized Ohm's law are discussed in Appendix A1.

Note that calling L_{MHD} and L_{EMHD} the normalization lengths in RMHD and EMHD, the inequality

$$\frac{\tau_W^*}{\tau_A^*} = \left(\frac{L_{\text{EMHD}}}{d_i}\right)\left(\frac{L_{\text{EMHD}}}{L_{\text{MHD}}}\right) \ll 1 \tag{6}$$

must hold since the characteristic quantities in EMHD must be much smaller than d_i and those of RMHD much larger than d_i.

3.1. Linear Dispersion Relations

From now on all spatial quantities, unless otherwise specified, are taken to be normalized either to the length a or to the length L if they appear with an "*". We focus on collisionless regimes where $S^{-1} = S_{\text{EMHD}}^{-1} = 0$ and will neglect viscous effects, whose role in MHD has been clarified recently by *Tenerani et al.* [2015a]. In addition, to further simplify the analysis, we start by setting $\rho_s = 0$ in equations (2)–(5). Because of the fact that both the (squared) electron skin depth and the Lundquist number weigh nonideal terms in Ohm's law which allow magnetic lines to reconnect (Appendix A1), and of other similarities which will be later discussed, let us introduce for future use the notations $\varepsilon_d \equiv d_e^2$ and $\varepsilon_s \equiv S^{-1}$. Then, after rescaling, we will write

$$\varepsilon_d^* = \varepsilon_d\left(\frac{a}{L}\right)^2, \qquad \varepsilon_s^* = \varepsilon_s\left(\frac{a}{L}\right). \tag{7}$$

After linearizing equations (2) and (3) around an equilibrium $\psi_0(x/a)$ with perturbations of the form $\sim e^{iky+\gamma t}$, analytic approximations to the dispersion relations in both RMHD and EMHD may be obtained by applying the boundary layer technique, as first shown by *Furth et al.* [1963].

Here we summarize the results valid in the two asymptotic regimes called large (LD) and small (SD) Δ', which, respectively, correspond to the internal kink and constant-ψ orderings [*Ara et al.*, 1978]. In RMHD such regimes are, respectively, defined by the conditions $\Delta'\delta > 1$ (LD) and $\Delta'\delta < 1$ (SD), where δ is the characteristic reconnection layer width. The instability parameter $\Delta' \equiv [\psi'_{\text{out}}(0^+) - \psi'_{\text{out}}(0^-)]/\psi_{\text{out}}(0)$, which in nonnormalized units has the inverse dimension of a length, is defined with ψ_{out} being the boundary layer solution of

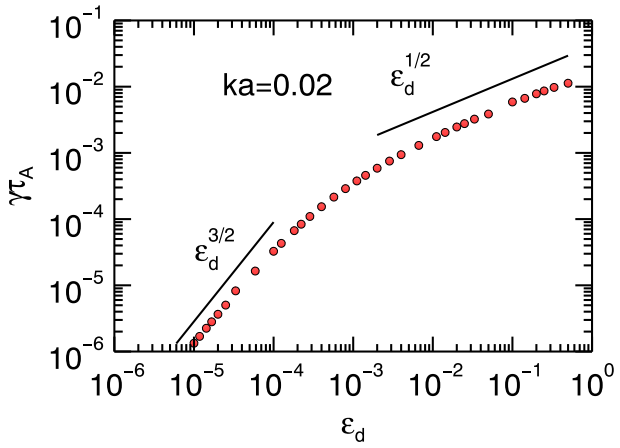

Figure 1. Scaling of $\gamma(\tilde{k})\tau_A$ in the RMHD regime as a function of d_e^2 for a fixed $\tilde{k}$. Here $\tilde{k} = k_M$ for $d_e^2 \simeq 2 \times 10^{-3}$ (lengths in units of a). The left and right asymptotes evidence the scalings of the small and large Δ' regimes, respectively.

equations (2) and (3) valid in the "outer" region, where the ideal MHD approximation holds. For the Harris pinch equilibrium, for example, $\Delta'(k) = 2(1/k - k)$ in units normalized to a. The inertial RMHD tearing dispersion relations become [see, e.g., *Porcelli*, 1991]

$$\text{RMHD} \begin{cases} \gamma_{LD}\tau_A = kd_e \\ \gamma_{SD}\tau_A = (C_1\Delta')^2 kd_e^3 \end{cases}, \tag{8}$$

where $C_1 \equiv \Gamma(1/4)/(2\pi\Gamma(3/4)) \simeq 0.4709$.

In EMHD, where the LD limit corresponds more properly to the condition $\gamma_{\text{LD}}/k \sim constant$, we consider the dispersion relations

$$\text{EMHD} \begin{cases} \gamma_{\text{LD}}\tau_W = C_2 kd_e^{\frac{2}{3}} \\ \gamma_{\text{SD}}\tau_W = \left(C_1\Delta'\right)^2 d_e^2 \end{cases}, \tag{9}$$

where $C_2 \equiv (2\Gamma^4(3/4))^{-1/3} \simeq 0.6053$. The γ_{LD} growth rate, evaluated by *Attico et al.* [2000] starting from an equilibrium given by $\psi_0(x) = x/a$ for $-a < x < a$ and $\psi_0(x) = 1$ for $|x| \geq a$, is considered the prototype for the more general "LD" EMHD dispersion relation for a generic sheared, even, $\psi_0(x)$ profile. The reason is that it is the only available expression obtained for this wavelength regime, and, with the same equilibrium, the general γ_{SD} dispersion relation first computed in [*Bulanov et al.*, 1992] and quoted in equation (9) is exactly recovered.

Figure 1 shows the scaling of the growth rate of a given unstable mode $\tilde{k}$ as a function of ε_d in the RMHD regime. Notice that the whole range of regimes from SD to LD is spanned by varying the value of d_e at given k. Indeed, since $\delta = \delta(k, \varepsilon_d)$, an interval in the ε_d parameter space such that $\Delta'(\tilde{k})\delta(\tilde{k}, \varepsilon_d)$ is smaller (SD), equal (γ_M; see section 4.1), or greater (LD) than unity always exists.

As a comment, note that almost ideal growth rates (saturating at $(\gamma_{\text{LD}}^{\text{EMHD}})^* \simeq 0.25(\tau_W^*)^{-1}$) are obtained in numerical integrations of the EMHD linear system at $0.1 \lesssim d_e < 1$ [*Del Sarto et al.*, 2005] for $L/a = 2\pi$ and $k^* = k = 1$. Such large values of d_e are not unreasonable in the collisionless EMHD regime, because of the constraint $d_e \ll a \ll d_i$ (now in dimensional units), which must be fulfilled by the equilibrium shear length. With such large values of the reconnection parameter, we are outside the realm of the asymptotic/boundary layer analysis, but for EMHD this is to be expected, since characteristic EMHD scale lengths must satisfy ℓ fulfill $d_e \ll \ell$ or, given that $d_i/d_e \simeq 42Z$ for an ion charge Z, $d_e \ll \ell \ll 42d_eZ$. Similarly, large growth rates are found in strongly resistive RMHD regimes $S^{-1} \gtrsim 0.01$, though these are normally of little interest. Discrepancies with analytical estimates from equations (7) and (8) suggest that at $\varepsilon_d \sim 0.01$ or equivalently $\varepsilon_S \sim 0.01$ the boundary layer approach for solving the tearing mode instability breaks down.

4. Results

4.1. Transition to the Inertial Ideal Regime

When $L/a \gg 1$, say, $L/a \gtrsim 20$ [*Velli and Hood*, 1989]—which will be the case when a scaling of the aspect ratio is considered in the ideal transition—it is necessary to focus directly on the fastest growing mode at

given parameter values, i.e., the mode k_M yielding the maximal growth rate γ_M. As noticed by *Battacharjee et al.* [2009], the latter can be estimated by imposing the condition $\gamma_{LD}(k_M) = \gamma_{SD}(k_M) \equiv \gamma_M$. Approximating $\Delta'(k_M) \simeq Kk_M^{-p}$, where K is a constant, from equations (8) and (9), we can estimate

$$\text{RMHD} \begin{cases} k_M \simeq (KC_1)^{\frac{1}{p}} d_e^{\frac{1}{p}} \\ \gamma_M \tau_A \simeq (KC_1)\, d_e^{\frac{1+p}{p}}, \end{cases} \tag{10}$$

$$\text{EMHD} \begin{cases} k_M \simeq \left(\frac{K^2 C_1^2}{C_2}\right)^{\frac{1}{1+2p}} d_e^{\frac{4}{3(1+2p)}} \\ \gamma_M \tau_W \simeq (KC_1 C_2^p)^{\frac{2}{1+2p}} d_e^{\frac{2}{3}\frac{3+2p}{1+2p}}. \end{cases} \tag{11}$$

Let us now apply the rescaling argument to evaluate, from equations (10) and (11) and from the definitions of τ_A and τ_W, the scaling of the most unstable mode when lengths are normalized to L. Neglecting the numerical coefficients in the parentheses of equations (10) and (11), we find in RMHD

$$k_M^* \simeq (\varepsilon_d^*)^{\frac{1}{2p}} \left(\frac{L}{a}\right)^{\frac{1+p}{p}} \qquad \gamma_M \tau_A^* \simeq (\varepsilon_d^*)^{\frac{1+p}{2p}} \left(\frac{L}{a}\right)^{\frac{1+2p}{p}}, \tag{12}$$

while in EMHD

$$k_M^* \simeq (\varepsilon_d^*)^{\frac{2}{3+6p}} \left(\frac{L}{a}\right)^{\frac{7+6p}{3+6p}} \qquad \gamma_M \tau_W^* \simeq (\varepsilon_d^*)^{\frac{3+2p}{3+6p}} \left(\frac{L}{a}\right)^{\frac{12+16p}{3+6p}}. \tag{13}$$

In RMHD, where $\psi'' \sim \psi/\delta^2$ and $\psi'' \sim \psi\Delta'/\delta_{SD}$ in the LD and SD regimes, respectively, it is immediate to verify by balancing $\psi \sim d_e^2 \psi''$ (cf. equation (2)) that $\delta_{LD} \sim d_e$ and $\delta_{SD} \sim \Delta' d_e^2$ whence we deduce using equation (12) that the fastest growing mode satisfies the condition $\Delta'(k_M)\delta_M(k_M) \sim 1$. The characteristic width of the reconnection layer for the most unstable RMHD mode therefore becomes

$$\delta_M \simeq d_e, \tag{14}$$

which, after rescaling, reads $\delta_M^* \simeq (\varepsilon_d^*)^{\frac{1}{2}}$.

The condition for ideal tearing is set by searching for the value of α such that when the critical aspect ratio $a_{IT}^* \equiv (a/L)_{IT} \sim (\varepsilon_d^*)^\alpha$ with $\alpha > 0$, γ_M^* becomes independent of $\varepsilon_d^* = (a_{IT}^*)^2 \varepsilon_d$. Imposing this, we find the exponent α both in RMHD and EMHD, respectively,

$$\alpha_d^{\text{RMHD}} = \frac{1+p}{2+4p}, \qquad \alpha_d^{\text{EMHD}} = \frac{3+2p}{12+16p}. \tag{15}$$

That is, referring the critical a_{IT}^* to each regime,

$$\left(\frac{a}{L}\right)_{\text{RMHD}} = \left(\frac{d_e}{L}\right)^{\frac{1+p}{1+2p}}, \quad \left(\frac{a}{L}\right)_{\text{EMHD}} = \left(\frac{d_e}{L}\right)^{\frac{3+2p}{6+8p}}. \tag{16}$$

In particular, for a Harris pinch equilibrium, which has $p = 1$, we find

$$\alpha_d^{\text{RMHD}} = \frac{1}{3}, \qquad \alpha_d^{\text{EMHD}} = \frac{5}{28} \simeq 0.1786. \tag{17}$$

A set of curves $\gamma(k)$ for different values of d_e along the RMHD threshold condition $(a/L)_{\text{RMHD}} = (\varepsilon_d^*)^{1/3}$, obtained by numerical integration of the eigenvalue problem with the Lentini-Pereyra algorithm [*Lentini and Pereyra*, 1974], are plotted in Figure 2a, while the corresponding graph for the EMHD regime is in Figure 2b. The independence of γ_M^* from d_e and its value of order unity, namely, $\simeq 0.39(\tau_A^*)^{-1}$ in RMHD and $\simeq 0.37(\tau_W^*)^{-1}$ in EMHD, are evidenced in both regimes. Referring to the example of the Harris pinch profile and assuming for EMHD the numerical threshold condition $(a/L)_{\text{EMHD}} = (\varepsilon_d^*)^{\frac{3}{16}}$, we then deduce the scalings of the threshold current sheet widths a with respect to d_e, which will be discussed in section 6

$$\left(\frac{a}{d_e}\right)_{\text{RMHD}} = \left(\frac{L}{d_e}\right)^{\frac{1}{3}}, \qquad \left(\frac{a}{d_e}\right)_{\text{EMHD}} = \left(\frac{L}{d_e}\right)^{\frac{5}{8}}. \tag{18}$$

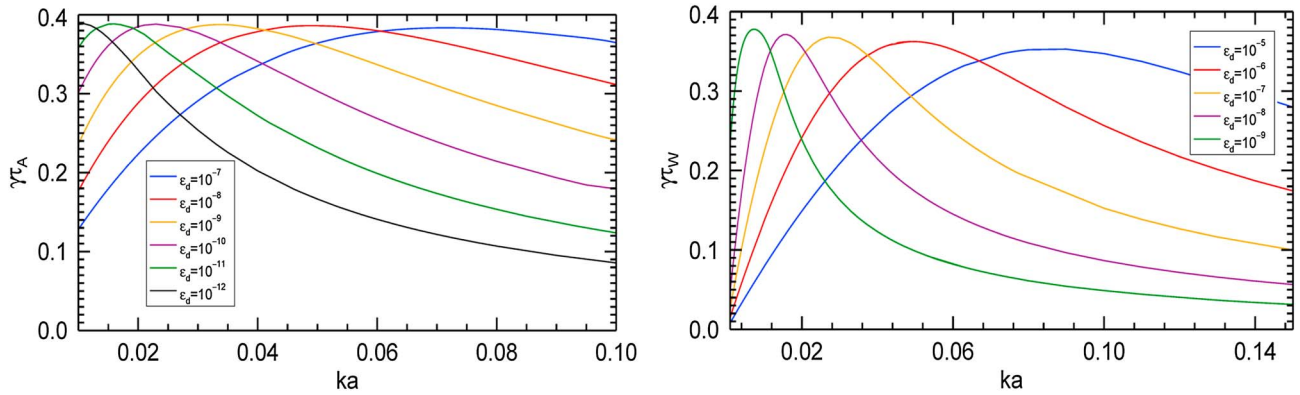

Figure 2. RMHD (left frame) and EMHD (right frame) dispersion relations $\gamma^* = \gamma^*(k^*, \varepsilon_d^*)$, computed for different values of d_e and represented as functions of k^*a^*. For each curve an aspect ratio was chosen, satisfying the threshold condition for a Harris pinch equilibrium, $a/L = (\varepsilon_d^*)^{1/3}$ in RMHD and $a/L = (\varepsilon_d^*)^{3/16}$ in EMHD. The d_e-independent maximum growth rates on each curve are $\gamma_M^* \tau_A^* \simeq 0.39$ in RMHD and $\gamma_M^* \tau_W^* \simeq 0.37$ in EMHD.

4.2. Kinetic Effects in the Transition to the Inertial Ideal Tearing: FLR Corrections

We now briefly discuss the role played by other kinetic effects important at the small spatial scales $a \ll L$ where the transition to ideal tearing takes place. We focus on FLR effects, which enter in the RMHD set of equations through gyrofluid corrections, an example of which is provided by the ρ_s term in equation (2).

It is well known that kinetic effects dominate collisionless tearing when the reconnection layer width becomes thinner than the ion Larmor radius, i.e., when $\delta \lesssim \rho_i$, where $\rho_i \equiv v_{\rm th}^i/\Omega_{ci}$ and $v_{\rm th}^i$ is the ion thermal velocity [*Drake and Lee*, 1977]. Kinetic tearing modes are affected by wave-particle resonances [*Coppi et al.*, 1966; *Laval et al.*, 1966; *Schindler*, 1974] and, generally speaking, by thermal features, which may be due to either initially multipeaked distributions [see, e.g., *Zeleney et al.*, 2008] or temperature anisotropies (see *Hewett et al.* [1988] for a gyrotropic case). When associated with an anisotropic electron pressure tensor, such as that expected in the vicinity of *X* points because of the flow shear [*Brackbill*, 2011; *Del Sarto et al.*, 2015], the latter are usually the dominant driving terms in quasi-collisionless reconnection [*Cai and Lee*, 1997]—cf. equation (A3). Under appropriate closure assumptions, a fluid framework suffices for this description [see, e.g., *Kutznesova and Hesse*, 1998; *Yin and Winske*, 2003; *Cassak et al.*, 2015, and references therein].

We speak of gyrofluid models when anisotropic effects are limited to the fluid inclusion of FLR corrections within a dominant gyrotropic dynamics. An example is given by equations (2) and (3) at $\rho_s \neq 0$ shown by *Pegoraro et al.* [2004] to give results in good agreement with those of a strong guide field, drift-kinetic model of reconnection. Ion-FLR effects, related to the ion sound Larmor radius by $\rho_i^2 = \rho_s^2 T_i/T_e$, can also be included in these models by making some closure assumption on the ion-kinetic response obtained from the transport equations. In the RMHD model we considered, ρ_i-related terms modify the Laplacian operator applied to the field φ in equation (3) [*Schep et al.*, 1994]. Different gyrofluid models are then available, but even those having different Hamiltonian properties—compared in *Waelbroeck et al.* [2009]—were shown to provide numerical results in remarkably good agreement (both in linear and nonlinear regimes) [*Grasso et al.*, 2010; *Del Sarto et al.*, 2011]. In particular, in a certain parameter range and regardless of the specific gyrofluid model considered, the theoretically predicted tearing mode scalings [*Pegoraro and Schep*, 1986; *Pegoraro et al.*, 1989; *Porcelli*, 1991] display a symmetric dependence on the two FLR effects, entering the dispersion relation only through powers of $\rho_\tau^2 = \rho_s^2 + \rho_i^2$. Even if appreciable discrepancies from these predictions are numerically measured as the ratio ρ_τ^2/d_e^2 increases [*Del Sarto et al.*, 2011], a good agreement is found at $\Delta' d_e \gg \min\{1, (d_e/\rho_\tau)^{1/3}\}$ [*Comisso et al.*, 2012].

In the "kinetic Alfvén" regime $\rho_\tau^2 > d_e^2$ (Appendix A1), *Comisso et al.* [2013] recently pointed out the existence of a maximum growth rate in the continuum spectrum limit (i.e., continuous k) of unstable tearing modes, corresponding, in our notation, to k_M. That dispersion relation can be obtained from equations (2) and (3) of the present paper, after the inclusion of small ion-FLR corrections. The generalization of their result for the Harris pinch case to generic equilibria is obtained as described in section 4.1, by starting from their equations (26) and (27) instead of our equation (8). We find

$$k_M \simeq d_e^{\frac{2}{3p}} \rho_\tau^{\frac{1}{3p}}, \qquad \gamma_M \tau_A \simeq d_e^{\frac{2+p}{3p}} \rho_\tau^{\frac{1+2p}{3p}}. \tag{19}$$

Table 1. Characteristic Plasma Parameters of Magnetized Plasma Environments Where Tearing Reconnection May Occur[a]

	Low Corona	Magnetotail	Tokamak		
	(Sun at $\sim 1R_\odot$)	(Central Plasma Sheet)	ITER	JET	MRX Device
Sources	I	II	III		IV
L	10^9-10^{10}	10^9-10^{10}	300	80	10–20
n_e	10^9-10^{10}	0.1	10^{14}	10^{13}	$(2-6)\times10^{13}$
B	10–100	10^{-4}	5.68×10^4	3.45×10^4	$(1-3)\times10^2$
T_e	86	10^3-10^4	2×10^4	3×10^3	5–15
$\varepsilon_S^* \equiv (S^{-1})^*$	$10^{-15}-10^{-12}$	$10^{-17}-10^{-15}$	10^{-11}	10^{-9}	$8\times10^{-4}-3\times10^{-2}$
$\underline{\varepsilon}_S^* \equiv (\underline{S}^{-1})^*$		$10^{-11}-10^{-10}$			
$\varepsilon_d^* \equiv (d_e/L)^2$	$10^{-19}-10^{-16}$	$10^{-8}-10^{-6}$	10^{-8}	10^{-6}	$10^{-5}-10^{-4}$

[a]Physical quantities are expressed in centimeter-gram-second units, and temperatures are expressed in eV. For magnetotail reconnection parameters, typical conditions in the plasma sheet during a substorm growth phase have been considered, and an effective Lundquist number $\underline{\varepsilon}_S^*$ has been evaluated from the anomalous resistivity, estimated from satellite data [*Eastwood et al.*, 2009] assuming wave-particle scattering on lower hybrid turbulence [*Coroniti*, 1985]. For tokamak devices the values are estimated from design (ITER) or measurements (JET) near to the $q = 1$ surface, whose circumference on a poloidal section, divided by 3 [*Waelbroeck*, 1993], gives an estimation of the typical reconnecting current sheet length, L. Source for the parameters, as labeled in the table's third row, are as follows: *Shibata and Magara* [2011] (I) ;*Angelopoulos et al.* [2014], *Eastwood et al.* [2009], *Sergeev et al.* [1993], and *Kivelson and Russell* [1995] (II); *Porcelli et al.* [1996] and *Rebut et al.* [1985] (III); and *Yamada et al.* [2014] (IV).

Then, applying the rescaling arguments, we obtain

$$\gamma_M \tau_A^* \simeq (\varepsilon_d^*)^{\frac{2+p}{6p}} (\rho_\tau^*)^{\frac{1+2p}{3p}} \left(\frac{L}{a}\right)^{\frac{1+2p}{p}}, \tag{20}$$

whence we deduce $\gamma_M^{\mathrm{FLR}} \tau_A^* \sim O(1)$ when

$$\left(\frac{a}{L}\right)_{\mathrm{FLR}} \sim (\varepsilon_d^*)^{\frac{1+p}{2+4p}} \left(\frac{\rho_\tau^*}{d_e^*}\right)^{\frac{1}{3}}. \tag{21}$$

We then see that depending on the value of the ratio ρ_τ/d_e, the inclusion of FLR corrections may imply an even larger critical aspect ratio for the transition to ideal tearing, with respect to the cold plasma limit. Indeed, if we now assume $\rho_\tau \simeq A d_e$ and we compare the IT threshold condition of equation (21) with that of equation (15) for the RMHD, we see that the two are related through $(a/L)_{\mathrm{FLR}} \sim A^{1/3}(a/L)_{\mathrm{RMHD}}$. Since usually $A > 1$ (e.g., typically $A \sim 10$ in tokamak plasmas and it may be even larger in the magnetosphere), this implies a broadening of the ideally unstable current sheet with respect to the cold plasma case, once kinetic effects are taken into account.

5. Discussion

5.1. Collisionless Ideal Tearing in Space, Solar, and Laboratory Plasmas

We now discuss how the IT model applies to various natural and laboratory environments. To compare the relative roles of electron inertia and resistivity, different plasma parameters, including ε_S^* and ε_d^*, are shown in Table 1.

We first note that the condition for purely collisionless, fluid reconnection ($S^{-1} = 0$) is given by $\gamma_d \tau_A \varepsilon_d \gg \varepsilon_S$, where γ_d is the growth rate in the purely inertia-driven regime. This condition is ever more readily satisfied when approaching the ideal regime ($a/L \ll 1$), where $\gamma_d \tau_A^* \to 1$ because the rescaling argument implies $\varepsilon_S/\varepsilon_d = (a/L)\varepsilon_S^*/\varepsilon_d^*$ (equations (7)). It follows that if $\varepsilon_S^*/\varepsilon_d^* \ll 1$, the IT limit corresponds to inertia-driven reconnection. Indeed, electron inertia, ε_d, enters in the the dispersion relation with a less favorable scaling with respect to resistivity, ε_S. For example, at $a/L \sim 1$ the estimations $\gamma_d \tau_A \sim \varepsilon_d^{1/2}$ (LD) and $\gamma_d \tau_A \sim \varepsilon_d^{3/2}$ (SD) imply inertial reconnection when $\varepsilon_d \gg \varepsilon_S^{2/3}$ and $\varepsilon_d \gg \varepsilon_S^{2/5}$, respectively.

In Figure 3 we show a numerical solution of equations (2) and (3) as a function of the a-normalized wave number for two cases: one with small and one with vanishing collisional resistivity, showing that no appreciable

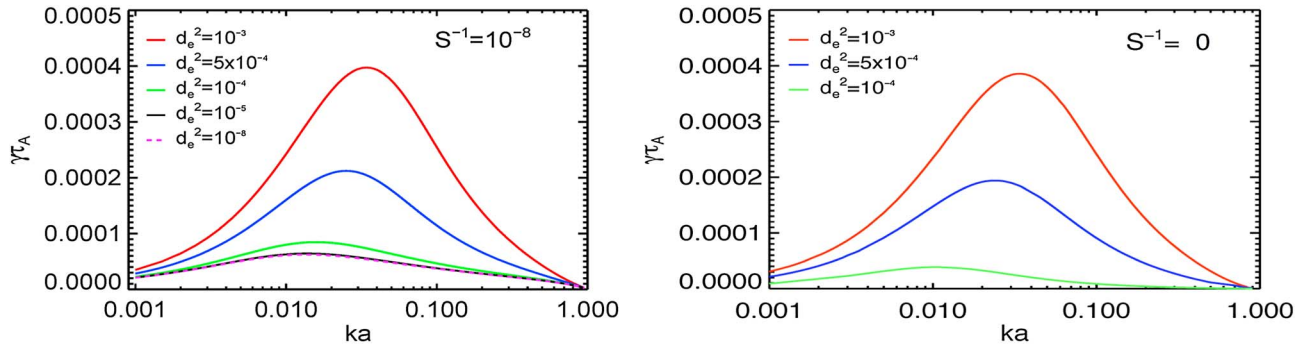

Figure 3. Dispersion relations γ versus k for different values of d_e and for (left) $S^{-1} = 10^{-8}$ and (right) $S^{-1} = 0$.

difference is observed in the inertial-resistive growth rates with $\varepsilon_s = 10^{-8}$ and $\varepsilon_d = 10^{-8}$–10^{-5} with $\varepsilon_s = 0$. Note that for this case only an implicit analytical expression is available [see, e.g., *Ottaviani and Porcelli*, 1995, equation (16)].

At higher values of S^{-1}, both the inertial and the resistive contributions to the fluid inertial-resistive growth rate become appreciable, and for $S^{-1} \gtrsim 10^{-6}$ the resistive contribution to the growth rate is relevant even for ε_d approaching unity.

The conclusions which can be drawn from Table 1 depend on the reconnection model assumed. For example, the RMHD equations (2) and (3) provide a satisfactory description of the local dynamics of single helicity reconnection modes in strong guide field plasmas and provide a first modeling of local field reversal configurations in solar loops too [*Velli and Hood*, 1989]. When temperature effects are included, they also apply to the slab kinetic Alfvén regime at $\beta_e > 2m_e/m_i$ (section 4.2). On this basis we see (Table 1) that fusion devices, for which $a \simeq L$, may operate in conditions in which the resistive contribution to tearing is not negligible even if $\varepsilon_s^*/\varepsilon_d^* \sim \varepsilon_s/\varepsilon_d \sim 10^{-2}$–$10^{-3}$ because of the smallness of $\gamma_d \tau_A^*$, which remains of the same order of $\gamma_d \tau_A \ll 1$. Solar loop reconnection would appear instead to be mostly resistivity driven.

Use of the IT reconnection scenario to understand the transition to instability of naturally occurring plasma configurations should take into account both more general equilibrium configurations as well as more complex geometries. The simplification of slab geometry adopted here neglects possible curvature effects and prevents coupling or competition with a variety of other instabilities which appear in more complex geometries, examples ranging from the ideal kink modes in solar loops [*Velli et al.*, 1990] or ballooning-interchange modes, both in tokamaks [*Coppi*, 1977] and in solar loops and arcades [*Velli et al.*, 1986, 1987].

For magnetospheric reconnection, even the geometry and structure of the relevant magnetic equilibria is unclear. Both in kinetic [*Galeev and Zelenyi*, 1976; *Lembege and Pellat*, 1982; *Pellat et al.*, 1991; *Brittnacher et al.*, 1994] and in fluid regimes [*Somov and Verneta*, 1988], tearing modes on a 1-D Harris-type current sheet are known to be stabilized once a uniform in-plane magnetic component normal to the neutral line (in the magnetotail its amplitude can be about 10% of the asymptotic reversing field) is present. The stabilization is affected by a gradient of this normal component and can be strongly reduced when 2-D magnetic configurations characterized by more than two spatial scales are considered [*Sitnov and Schindler*, 2010]. An example is given by a localized maximum in the normal field [*Pritchett*, 2015]. Second, the essential features of the reconnection mechanism itself are debated: here wave-particle scattering dominates over Coulomb collisions (see Table 1) and kinetic effects are expected to prevail. The latter, however, combine among themselves (e.g., Landau resonances with non-Maxwellian features of the distribution function [*Zeleney et al.*, 2008; *Hewett et al.*, 1988] or with temperature differences between ions and electrons [*Sitnov et al.*, 2002]) to affect tearing growth rates and thresholds. Moreover, some of these kinetic effects (pressure anisotropies) can be fully described with fluid models (section 4.2). In this regard, it is interesting to note that, even results obtained from the quite idealized, "cold" EMHD, equations (4) and (5), have been compared, with qualitative and partially quantitative agreements, to Cluster measurements of magnetotail reconnection [*Jain and Sharma*, 2015].

The above discussion argues in favor of an extension of the IT analysis to more general equilibrium configurations tailored to specific problems, a project which goes beyond this present initial work: the goal of the models presented here (section 3) is to provide a reasonably simple starting point still sufficiently general to

introduce the extension of IT to less idealized equilibrium configurations and to fully kinetic tearing regimes (see, e.g., *Daughton* [1999], *Daughton et al.* [2005, 2011], *Quest et al.* [2010], and the aforementioned references). In fact, regardless of the specific collisionless reconnection mechanism at play, the results discussed in section 4 and in particular the existence of a critical aspect ratio $(a/L)_{IT}$ marking the boundary between slowly unstable and violently unstable current sheets can be adapted to other collisionless tearing regimes, similar to our discussion in section 4.2: the key points to determine the transition to fast reconnection lie in the rescaling argument of the specific a-normalized growth rate under examination, followed by assuming the condition $\gamma\tau^* \sim O(1)$ as the physical limit which fixes the threshold value $(a/L)_{IT}$.

All reconnection mechanisms, fluid or kinetic, share the common point of being driven by nonideal effects and thus of having dominant tearing growth rates (at sufficiently large aspect ratio) scaling as positive powers of some microscopic parameters. Call ε the generic dimensionless parameter including all nonideal contributions with their appropriate power or product of powers, so that $\gamma\tau \sim \varepsilon$. The ideal limit disallows a reconnecting instability implying $\gamma\tau \to 0$ and $\varepsilon \to 0$ as $a \to \infty$. This requires that ε must scale as some *negative* power, say $-\sigma$, of the equilibrium scale length. Upon renormalization to a macroscopic scale L therefore $\varepsilon^* = (a/L)^\sigma \varepsilon$. If we now take the inverse limit of quasi singular current sheets and assume as usual that the reference time is the corresponding Alfvén time, we obtain $\gamma\tau_A^*(a/L) \sim \varepsilon^*(L/a)^\sigma$, and by an appropriate scaling of the inverse aspect ratio with ε^* we find a trigger threshold aspect ratio for IT, which scales as the power $0 < 1/(1+\sigma) < 1$ of ε^*,

$$\left(\frac{a}{L}\right)_{IT} \sim (\varepsilon^*)^\alpha, \quad \alpha = \frac{1}{1+\sigma}, \quad \sigma > 0. \tag{22}$$

Writing, for example, the classical dispersion relation of the dominant ion-kinetic tearing mode [*Schindler*, 1974] in our notation, $\gamma\tau_A \sim (\pi/8)^{1/2}\rho_i^{5/2}/(a^{3/2}d_i)$, with reference to equation (22), we identify $\sigma = 3/2$ for $\varepsilon = \rho_i^{5/2}/(a^{3/2}d_i)$. This leads to the critical aspect ratio $(a/L)_{IT} \sim \rho_i/(L^{3/5}d_i^{2/5})$ with $\alpha = 2/5$. Let us assume for simplicity that in the magnetotail $T_i \sim T_e = 5 \times 10^3$ eV. Though this may not be too appropriate, as typically $T_i > T_e$ [see *Sitnov et al.*, 2002, and references therein], it illustrates our arguments well, since we are considering the most simplified model in which other effects on the growth rate and threshold of ion-kinetic tearing are neglected. From Table 1 we then obtain $\rho_i \sim d_i \sim 7 \times 10^7$ cm. This corresponds to critical shear values $a_{IT} \sim (2-5) \times 10^8$ cm for $L \sim 10^9 - 10^{10}$ cm, thus suggesting that at typical magnetotail parameters it is possible for the ion-kinetic tearing to develop in the IT regime.

5.2. Ideal Tearing and Stability of Steady State Reconnecting Current Sheets in the Collisionless Regime

Both in MHD [*Wesson*, 1990] and in EMHD [*Bulanov et al.*, 1992; *Avinash et al.*, 1998], the reconnection rate of a steady state current sheet has been evaluated in the collisionless regime, as a generalization of the classic Sweet-Parker configuration. In both cases the same scaling in ε_d of the stationary Sweet-Parker-like reconnection rate τ_{SP}^{-1} was obtained with respect to the respective normalization times, $(\tau_{SP}^{EMHD})^{-1}\tau_w^* \sim (\varepsilon_d^*)^{1/2}$ and $(\tau_{SP}^{RMHD})^{-1}\tau_A^* \sim (\varepsilon_d^*)^{1/2}$. This implies that both in collisionless RMHD and EMHD, the aspect ratio scaling of a steady current sheet of length L is $(a/L)_{SP} \sim (\varepsilon_d^*)^{1/2}$. By comparing the scaling of this ratio with the threshold conditions for the onset of ideal tearing (equation (15)) the same qualitative behavior, though with different scalings, is evidenced in both RMHD and EMHD. In RMHD the width of the steady reconnecting layer corresponds to a much thinner current sheet than that which is unstable to ideal tearing: at a given length L, the collisionless Sweet-Parker sheet width, a_{SP}, is related to the ideal tearing unstable one, a_{IT}, by the relation $a_{SP}^* \simeq (a_{IT}^*)^{(1+2p)/(1+p)}$. Using the same reasoning, we can estimate from equation (15) $a_{SP}^* \simeq (a_{IT}^*)^{(6+8p)/(3+2p)}$ for EMHD. If we now neglect the effect of the flow along the neutral line on the growth rate (cf. also *Tenerani et al.* [2015b], for why flows may be neglected), this means that both in RMHD and EMHD a collisionless Sweet-Parker-type current sheet is always unstable on ideal time scales.

5.3. "Secondary" Ideal Tearing and Explosive Reconnection

The above discussions demonstrate that the rescaling argument at the basis of ideal tearing may provide a fairly general paradigm to describe explosive growth rate increases. Consider now what is observed in the nonlinear stage of simulations of reconnection at L/a not much larger than unity [*Ali et al.*, 2014; *Biancalani and Scott*, 2012; *Yu et al.*, 2014], when an X point collapses into two Y points and the current sheet between the two becomes tearing unstable, eventually leading to what has been interpreted as the plasmoid chain instability.

Let be L_Y the length and a_Y the width of a secondary current sheet between two Y points, generated in the nonlinear stage of the tearing of a current sheet with inverse aspect ratio a/L. If the dynamics were analyzed in terms of the classical tearing mode, growth rates would refer to the length a_Y, whereas we now need to label with "$\tilde{..}$" the quantities normalized to L_Y, since the latter now plays the role of macroscopic length for secondary dynamics (cf. section 2). Even considering a primary tearing mode with $L/a \gtrsim 1$, the secondary current sheet develops with a much smaller thickness (corresponding to the singular layer thickness of the original tearing instability) so that we focus on the fastest growing tearing mode at the given aspect ratio L_Y/a_Y: accounting for FLR effects, the renormalized most unstable, tearing mode growth rate on the secondary current sheet is given by (cf. section 4.2)

$$\gamma_M^{\mathrm{FLR}}\tilde{\tau}_A \sim \tilde{\varepsilon}_d^{\frac{2+p}{6p}}\tilde{\rho}_\tau^{\frac{1+2p}{3p}}\left(\frac{L_Y}{a_Y}\right)^{\frac{1+2p}{p}}. \tag{23}$$

Analogously, we can rewrite in the corresponding resistive inviscid and viscous, high-Prandtl number RMHD regimes (respectively, discussed in *Pucci and Velli* [2014] and *Tenerani et al.* [2015a, 2015b])

$$\gamma_M^{\mathrm{res}}\tilde{\tau}_A \sim \tilde{\varepsilon}_S^{\frac{1+p}{1+3p}}\left(\frac{L_Y}{a_Y}\right)^{\frac{2+4p}{1+3p}}, \tag{24}$$

$$\gamma_M^{\mathrm{visc}}\tilde{\tau}_A \sim \tilde{\varepsilon}_S^{\frac{1+2p}{1+3p}}\tilde{R}^{\frac{p}{1+3p}}\left(\frac{L_Y}{a_Y}\right)^{\frac{2+4p}{1+3p}}. \tag{25}$$

Note that the occurrence of a secondary, ideal tearing mode developing as a consequence of a primary tearing in a large aspect ratio current sheet in the resistive RMHD regime was first numerically evidenced by *Landi et al.* [2015] and further discussed in depth in *Tenerani et al.* [2015b]. However, for the discussion here the primary tearing mode has $a \sim L$, so the primary reconnection rate cannot be estimated with that of the most unstable mode γ_M; rather, the specific LD or SD regime in which the unstable wave number falls must be taken into account. Comparing such a primary reconnection rate to the secondary one, as estimated from equations (23)–(25), we immediately recognize that even before the ideal tearing threshold is reached, the rescaling argument predicts an increase in the growth rate, *measured with respect to the primary mode macroscopic scale L*, by some positive power of $(L_Y/a_Y) > 1$ times some positive power of $(L/L_Y) > 1$. Comparing equations (23)–(25), we see that for equal equilibrium profiles (same $p \geq 1$), such an increase is relatively more important in the inertia-driven FLR regime.

To give a quantitative example, consider the RMHD-FLR regime supposing primary reconnection to develop on a current sheet described by the equilibrium used by *Comisso et al.* [2013], assuming an aspect ratio so close to unity that a single primary mode m_0 (i.e., $k_0 = 2\pi m_0/L$) is excited in the SD, constant-ψ regime, in the whole range of parameters in which d_e and ρ_τ are varied ($\Delta'\rho_\tau^{\frac{1}{3}} d_e^{\frac{2}{3}} < 1$). The primary tearing mode [see, e.g., *Comisso et al.*, 2013, equation (27)], once rescaled to L, grows with

$$\gamma_I\tau_A^* \simeq k_0^*(\varepsilon_d^*)^{\frac{1}{2}}\rho_\tau^*(\Delta')^*\left(\frac{L}{a}\right), \tag{26}$$

with some $(\Delta'(k_0^*))^*$ of order unity. For the secondary mode we may now use equation (23) expressed again in terms of the scale L. Assuming for simplicity (but with no loss of generality) that the secondary current sheet resembles a Harris pinch profile so to specify $p = 1$,

$$\gamma_{II}\tau_A^* \sim (\varepsilon_d^*)^{\frac{1}{2}}\rho_\tau^*\left(\frac{L}{a_Y}\right)^3. \tag{27}$$

A dominant increase of the reconnection rate is therefore provided by the ratio $L/a_Y \gg 1$. In particular, in this example we obtain

$$\frac{\gamma_{II}^*}{\gamma_I^*} \sim \frac{1}{k_0^*(\Delta')^*}\left(\frac{a}{a_Y}\right)\left(\frac{L}{a_Y}\right)^2. \tag{28}$$

Of course, a more detailed analysis would be required to verify whether the rescaling argument summarized by equations (23)–(25) and the corresponding threshold conditions for the ideal tearing suffice to explain the explosive reconnection regimes observed in the above mentioned numerical studies. However, the qualitative considerations about the scalings provided in Figure 3 of *Biancalani and Scott* [2011] and in Figure 2 of *Biancalani and Scott* [2012] seem encouraging. Because of the normalization assumed in these articles, the increase of the growth rates with decreasing plasma β implies for the linear growth rate a scaling $\gamma_l \tau_A^* \sim d_e$ and for the nonlinear one a scaling $\gamma_{nl} \tau_A^* \sim d_e^0$ at fixed ρ_s, thus suggesting (cf. equations (19) and (23) for $p = 1$) that an ideal tearing regime was observed in the nonlinear stage of the simulations discussed by *Biancalani and Scott* [2012]. Future studies will elucidate whether the explosive reconnection predicted by equation (23) and that studied in *Biancalani and Scott* [2012] are effectively the same phenomenon.

5.4. Implications for Turbulent Reconnection

In concluding this section, we note that the nonlinear reconnection rate increase previously discussed can be relevant to the magnetic energy dissipation rate in high-Reynolds number turbulence, first investigated in a purely resistive regime by *Matthaeus and Lamkin* [1985] and recently rediscussed by *Wan et al.* [2013]. The results of *Wan et al.* [2013] suggest that a prominent role in the mean square, turbulent, global reconnection rate is played by the reconnection rate at each of the X points, which develop in current sheets generated by turbulent convective motions and whose number increases with increasing S^*. In this nonlinear regime multiple modes may interact, something which is true in the nonlinear evolution of a single sheet as well [*Landi et al.*, 2015; *Tenerani et al.*, 2015b], and it is not necessarily the fastest growing mode that dominates the energetics. However, as seen also in *Tenerani et al.* [2015b], the number of X points formed does seem to be related to the fastest modes unstable on secondary, elongated, collapsed sheets, and these do increase consistently with increasing S^*—a detailed analysis and comparison with fully turbulent simulations would merit a paper in its own right. The results of *Wan et al.* [2013] therefore might well be consistent with the generation of secondary current sheets out of the collapse of X points due to tearing instabilities that grow on top of primary current sheets formed in the turbulent evolution of the flow. In the purely resistive case ($\varepsilon^* = (S^*)^{-1}$) this should be related to the scaling $\sim (S^*)^{3/2}$ of the number of X points in a 2-D simulation box of fixed area, found by *Wan et al.* [2013] in the nonlinear turbulent cascade, but a similar behavior, characterized by an increase of the number of reconnection sites while approaching the ideal limit $\varepsilon^* \to 0$, should also be expected when ε^* is due to inertial and possibly FLR effects. Therefore, similar to what is observed in the high-Reynolds number dissipative case, an overall increase of the inertia-driven turbulent reconnection rate could be expected at the decrease of d_e/L because of the reconnection rate increase related to the nonlinearly generated current sheets, as discussed in section 5.3. This picture naturally might change dramatically when going to three dimensions because of the further richness provided by secondary kinking instabilities: all this deserves a further dedicated investigation program.

6. Summary

We have extended the analysis of *Pucci and Velli* [2014] to collisionless regimes, both in RMHD and EMHD, by providing the scaling threshold values $(a/L)_{IT} \sim (d_e^2/L^2)^{\alpha}$ at which a current sheet will transition to tearing on the ideal macroscopic time scale of the model. For the Harris pinch equilibrium profile the exponents measured after numerical solution of the eigenvalue problem are $\alpha_d^{RMHD} = 1/3$ and $\alpha_d^{EMHD} \simeq 3/16$, in excellent agreement with the analytical estimates obtained starting from the SD and LD dispersion relations. In RMHD, FLR corrections typically reduce the width of the critical sheet for the transition to ideal tearing. In the parameter range $\Delta' d_e \gg \min[1, (d_e/\rho_\tau)^{1/3}]$ and for the Harris pinch case, the inverse aspect ratio becomes $(a/L)_{FLR} \sim (\varepsilon_d^*)^{1/6} (\rho_\tau^*)^{1/3}$, instead of $(a/L)_{RMHD} \sim (\varepsilon_d^*)^{1/3}$ in the $\rho_s = 0$ limit. Since this implies a broadening of the critical reconnection current layer by a factor $(d_e^*)^{-1/3} (\rho_\tau^*)^{1/3} \sim A^{1/3}$, when $\rho_\tau \simeq A d_e$ with $A > 1$, as is usually the case, FLR effects are expected to correspondingly lower the instability threshold.

The collisionless IT model has been applied to discuss the instability of steady collisionless reconnecting current sheets, which, just as in the resistive case, should not be observable if they are unstable to inertia-driven tearing modes on ideal time scales. We note, however, that the IT threshold current sheet, found to be thinner in RMHD than in EMHD (equations (18)), leaves the open question of how the Alfvénic and whistler-dominated frequency regimes relate to the Hall-MHD framework, which in principle encompasses both in two opposite limits (see Appendix A2). We are currently analyzing this question with a dedicated study.

We have also pointed out the relevance and importance of inertia-driven versus resistive reconnection: the condition $S^{-1} \gg d_e^2 \gamma$ provides a stringent constraint on when resistivity may be neglected which is often overlooked, for example, when applying Vlasov models of reconnection to tokamak plasmas.

We have finally discussed how the rescaling argument at the basis of the IT model may explain the "explosive" reconnection rate increase observed during the nonlinear stage of primary reconnection events, as secondary elongated current sheets are generated during the collapse of an *X* point [*Ali et al.*, 2014; *Biancalani and Scott*, 2012; *Loureiro et al.*, 2005]. The IT regime may thus be in principle achieved also during secondary reconnection events involving the thin, elongated current layers nonlinearly generated by classical tearing processes [*Ottaviani and Porcelli*, 1993] or in kinetic turbulence [*Servidio et al.*, 2012]. Notice that large aspect ratio current layers are generally expected to develop because of the "exponentiation" of neighboring magnetic field lines [*Boozer*, 2012], and evidence of such exponential thinning of current sheets was recently provided, in the coronal heating context, by the numerical 3-D simulations of *Rappazzo and Parker* [2013]. This model therefore provides a promising key to interpret reconnection rates, which both in laboratory and astrophysics are — at least indirectly — observed to be orders of magnitude faster than what is predicted by the CT theory.

The simplicity of the rescaling argument at the basis of the IT model should not betray its nontrivial reach. The dominant trend of recent research on magnetic reconnection, aiming at predicting almost ideal reconnection rates, focuses indeed on the role played by kinetic processes and secondary instabilities, whereas the model first considered by *Pucci and Velli* [2014] has the appealing feature of relying on simple and well-known results. Besides, by being in principle extensible to any tearing reconnection rate regardless of the driving mechanism involved (section 5.1), it provides a general model for triggering fast reconnection, both in fluid and kinetic collisionless regimes, based on a critical aspect ratio $(a/L)_{IT}$ scaling as some small fractional positive power of the microscopic parameters.

Appendix A: Slab Geometry Equations From the Two-Fluids and From the Extended Hall-MHD Models

A1. Discussion of the Model Equations

Equations (2) – (5) are derived with different approximations from the electron and ion momentum equations, which we write here below, nondimensionalized using the equilibrium scale length a and the Alfvén time τ_A (and the electric field normalized to a fraction V_A/c of the magnetic field)

$$d_e^2 \left(\frac{\partial \boldsymbol{u}_e}{\partial t} + \boldsymbol{u}_e \cdot \boldsymbol{\nabla} \boldsymbol{u}_e \right) = -d_i \left(\boldsymbol{E} + \mathbf{u}_e \times \boldsymbol{B} - \frac{\boldsymbol{J}}{S} \right) - \rho_s^2 \frac{\boldsymbol{\nabla} \cdot \boldsymbol{\Pi}_e}{n_e}, \tag{A1}$$

$$d_i^2 \left(\frac{\partial \boldsymbol{u}_i}{\partial t} + \boldsymbol{u}_i \cdot \boldsymbol{\nabla} \boldsymbol{u}_i \right) = d_i \left(\boldsymbol{E} + \mathbf{u}_i \times \boldsymbol{B} - \frac{\boldsymbol{J}}{S} \right) - \rho_s^2 \frac{\boldsymbol{\nabla} \cdot \boldsymbol{\Pi}_i}{n_i}. \tag{A2}$$

The kinetic pressure has been normalized to a reference value P_0 for the electron plasma pressure leading to the factor ρ_s^2 in front of the ion pressure force in equation (A2), even though the ion thermal Larmor radius is $\rho_i = (T_i/T_e)^{1/2} \rho_s$. As discussed in *Del Sarto et al.* [2006] for the purely collisionless regime, equations (2) – (5) may be indeed obtained, under appropriate approximations and closures for the pressure tensors (and after renormalization to τ_w for the EMHD equations), from equations (A1) and (A2) coupled with Maxwell's equations using quasi-neutrality, $n_e = n_i$. Such an approach is essentially the one via which electron inertia effects were first included in reconnection models in the full MHD [*Coppi*, 1964a, 1964b] and RMHD frameworks [*Schep et al.*, 1994]. Within this approach, inclusion of resistive diffusion S^{-1} is straightforward, and the perpendicular ion-ion viscosity too can be retained in the form given in equation (3) if the hypothesis of a strong guide field is also assumed (for a recent discussion see *Tenerani et al.* [2015a]). Derivation of the EMHD equations follows simply from equations (4) and (5), since ion dynamics is completely neglected [*Kingsep et al.*, 1990].

It can be verified that both equations (2) and (4) represent the z component of electron momentum equation (equation A1) in the RMHD and EMHD regimes, respectively, ψ and $-\nabla^2 \psi$ expressing the z component of the vector potential $\boldsymbol{A}$ and of the electron current density $\boldsymbol{J}$.

In RMHD, the ρ_s^2 contribution on the right-hand side of equation (2) expresses thermal effects related to electron compressibility along magnetic field lines [see, e.g., *Kleva et al.*, 1995; *Grasso et al.*, 1999]: in the usual,

strong guide field limit, b, is completely neglected since $b \sim \epsilon^2$ with $\epsilon \equiv |\nabla\psi|/B_z \ll 1$, and to leading order ($\sim \epsilon$) both $\boldsymbol{u}_e$ and $\boldsymbol{u}_i$ are given by the incompressible $\boldsymbol{E}\times\boldsymbol{B}$ drift velocity. As a consequence, the stream function φ corresponds to the normalized electrostatic potential, while the ρ_s^2 term appears in the electron momentum equation as a result of the diamagnetic corrections to $\boldsymbol{u}_e$ in the Lorentz force and the z component of the gyrotropic electron pressure tensor [*Schep et al.*, 1994]. For this reason this term is considered to be an FLR-type contribution. However, the cancelation between the diamagnetic drift contribution to the z component of $\boldsymbol{u}_e \cdot \nabla \boldsymbol{u}_e$ and the z component of the gyrotropic pressure tensor is required in the derivation only if we do not order ρ_s and d_e with respect to ϵ; in that case equations (2) and (3) contain terms up to the second order in ϵ. If instead we remember that in the slab, strong guide field, RMHD ordering, $\beta_e \sim \epsilon$ and that $\rho_s^2 = \beta_e d_i^2/2$, then we may order $\rho_s^2 \sim d_e^2 \sim \epsilon$. This is sufficient to reobtain equations (2) and (3) even by assuming a scalar electron pressure tensor, neglecting contributions of order ϵ^4 or higher, since from $\boldsymbol{u}_{e,\perp} \simeq \boldsymbol{E}\times\boldsymbol{B}/B^2 + \boldsymbol{\nabla} P_e \times \boldsymbol{B}/(eB^2)$ we would obtain $(\boldsymbol{u}_e \times \boldsymbol{B}) \cdot \boldsymbol{e}_z = [\varphi - \rho_s^2 U, \psi]$; our equations will now retain terms up to ϵ^3. The ordering $\beta_e \sim d_e^2 \sim \epsilon$, that is $\beta_e \sim m_e/m_i$, is in principle consistent with the fluid description of collisionless reconnection as Landau resonances can dominate at $\beta_e > (m_e/m_i)^{1/2}$ [see, e.g., *Zeleney and Artemyev*, 2013]. We, however, recall that thanks to consistent description of the normal mode dispersion relations in the respective limits, the finite-temperature RMHD equations are applied both in the "inertial" regime $\beta_e \ll 2m_e/m_i$ and in the opposite kinetic Alfvèn regime $\rho_i^2 + \rho_s^2 \gg d_e^2$, equivalent to $\beta_e \gg 2m_e/m_i$ [see *Grasso et al.*, 2010]. In the latter ion-particle resonances are assumed as negligible at inverse time scales such that $|\omega| \gg k_{||} v_{\mathrm{th}}^i$, with ω complex mode frequency and $k_{||}$ wave vector parallel to the magnetic field, and an isothermal closure is a posteriori assumed [*Ottaviani and Porcelli*, 1995].

In EMHD, instead, the convection velocity field (i.e., $\boldsymbol{u}_\perp^e$) appearing in the second term of equation (4) is due to the magnetic field component b, since the current density is carried by electrons only, which drive the dynamics through $\boldsymbol{u}_e \propto \boldsymbol{J} \propto \boldsymbol{\nabla}\times\boldsymbol{B}$ in the incompressible regime that we consider here. As a consequence, b acts as a stream function for the in-plane electron dynamics, and resistivity, when included, enters also in the equivalent of the vorticity equation. For the same reason, the in-plane components of the electron momentum equation, taken in the polytropic, incompressible limit, suffice to close the system of EMHD equations: equation (5) is the z component of the rotational of equation (A1), and the field W is proportional to the z component of the electron generalized vorticity, defined by the curl of the electron fluid canonical momentum $\boldsymbol{\nabla}\times(\boldsymbol{u}_e + e\boldsymbol{A}/(m_e c))$.

The EMHD equation for the electron generalized vorticity is mirrored in RMHD by the equation for the fluid vorticity alone (equation (3)), of which $\nabla^2\varphi$ represents the z component [see also *Rogers et al.*, 2001]. This happens because in the Alfvénic frequency range the plasma moves at the bulk velocity $\boldsymbol{U} \simeq \boldsymbol{u}_i + O(m_e/m_i)$): equation (3) is therefore the curl of equation (A2), under the assumption of incompressibility, which allows expression of the perpendicular fluid velocity in terms of the stream function φ. If the plasma fluid is assumed to be incompressible but without imposing the strong guide field condition, this function cannot be interpreted as the electrostatic potential. With no guide field, however, a separate analysis would be required to include ρ_s^2-type contributions. The delicate point about the applicability of equations (2)–(5) lies indeed in the validity of the incompressibility assumption and in its relationship with the ordering of the parallel fluctuations of the magnetic field, which weighs the importance of Hall's term in Ohm's law discussed below.

A2. Comparison With the Generalized Ohm's Law and Hall's Term

Since reconnection models are usually discussed in relation to the nonideal terms in the generalized Ohm's law rather than in the framework of the full two-fluid equations for ions and electrons, we briefly discuss it here. Written with respect to the average plasma velocity $\boldsymbol{U}$, the standard textbook form is obtained by combining equations (A1) and (A2) [see, e.g., *Krall and Trivelpiece*, 1973, p. 91] while neglecting $O(m_e/m_i)$ corrections

$$\boldsymbol{E} + \boldsymbol{U}\times\boldsymbol{B} = d_i \frac{\boldsymbol{J}\times\boldsymbol{B}}{n} + S^{-1}\boldsymbol{J} + \frac{d_e^2}{n}\left\{\frac{\partial \boldsymbol{J}}{\partial t} + \boldsymbol{\nabla}\cdot\left(\boldsymbol{U}\boldsymbol{J} + \boldsymbol{J}\boldsymbol{U} - d_i\frac{\boldsymbol{J}\boldsymbol{J}}{n}\right)\right\} - \frac{\rho_s^2}{d_i}\frac{\boldsymbol{\nabla}\cdot\boldsymbol{\Pi}_e}{n}, \tag{A3}$$

where lengths have been normalized to a and times to τ_A. $n = n_e = n_i$ is the average plasma density, and $\boldsymbol{\Pi}_e$ is the electron pressure tensor of equation (A1), measured in the electron rest frame. The ion pressure tensor contribution is neglected since it is $O(m_e/m_i)$ smaller when the temperatures of the two species are comparable. Note that it has been recently shown by *Kimura and Morrison* [2014] that the (often neglected)

term $\nabla \cdot (\boldsymbol{JJ}/n)$ is necessary to respect energy conservation of the one-fluid system in the collisionless limit ($S^{-1} = 0$).

The generalized Ohm's law is essentially the rewriting of the electron momentum equation with respect to $\boldsymbol{U}$ and $\boldsymbol{J}$ that replace $\boldsymbol{u}_e$. We then recognize the essential difference between the dynamics of the bulk plasma and magnetic field and the role that the Hall term $\boldsymbol{J}\times\boldsymbol{B}$ has in the latter: while the plasma always moves at the fluid velocity of ions, the magnetic field (with the rotational of equation (A3)) is dragged by the fluid velocity of the electrons, $\boldsymbol{u}_e = (\boldsymbol{U} - d_i\boldsymbol{J}/n)$. In particular, the term $\boldsymbol{u}_e\times\boldsymbol{B}$ describes the convection of magnetic field lines by the electron fluid in the collisionless limit neglecting electron inertia. As well known [*Fruchtman and Maron*, 1991], the RMHD and EMHD sets of equations for slab reconnection without electron temperature effects may be therefore seen as two extreme limits with respect to the Hall term (d_i term), in Ohm's law: the RMHD regime described by equations (2) and (3) at $\rho_s = 0$ corresponds to neglecting Hall's term entirely, whereas the EMHD framework is recovered when the fluid dynamics is restricted to electrons only ($\boldsymbol{U} \simeq \boldsymbol{u}_i \simeq 0$), which is at scales $\ell \ll d_i$ and $\Omega_i \lesssim \omega \ll \Omega_e$, so that equation (A3) becomes the only relevant equation for our fluid system. It is, however, interesting to remark that in the strong guide field ordering, both ions and electrons in-plane velocities are equal at the leading order in ϵ to the $\boldsymbol{E}\times\boldsymbol{B}$ drift. By direct comparison of the z component of $\boldsymbol{u}_e\times\boldsymbol{B} = (\boldsymbol{U} - d_i\boldsymbol{J}/n)\times\boldsymbol{B}$ with $[\varphi - \rho_s^2 U, \psi]$ (cf. previous section), it is immediate to recognize that the Hall term survives in the ordering with $\rho_s^2 \sim \epsilon$ through the diamagnetic drift contribution to $\boldsymbol{u}_{e,\perp}$, $\rho_s^2[U,\psi] = d_i(\boldsymbol{J}\times\boldsymbol{B})\cdot\boldsymbol{e}_z/n$. This expresses the balance between kinetic and magnetic pressure forces not only at equilibrium but also for the perturbations.

When Hall's term is retained while still considering the bulk plasma response to field evolution (i.e., the ion momentum equation is not neglected, so that $\boldsymbol{J} \neq -ne\boldsymbol{u}_e$), an intermediate regime is entered, sometimes called "Hall-mediated reconnection" (HMR) or even "whistler-mediated reconnection" [*Mandt et al.*, 1994]. This should not be confused with the EMHD regime of equations (4) and (5), though there has been some ambiguous notation for different regimes in the past—also note that in some works, what we here name (resistive) HMR was even referred to as the "collisionless reconnection" regime [see, e.g., *Zweibel and Yamada*, 2009], due to the weak dependence on S found in the Hall-dominated reconnection rate [see, e.g., *Birn et al.*, 2001]. The HMR- and whistler-mediated reconnection regimes are not of concern in this paper, since they cannot be recovered in the framework of two-field models. The decoupling of ion and electron motions at the ion inertial scale (i.e., for $\ell \lesssim d_i$) requires more than two scalar fields to be retained to account for two-fluid effects (also notice that equations (2)–(5) do not contain d_i as a characteristic scale length). As discussed by *Fruchtman and Strauss* [1993], first, and more recently by *Bian and Vekstein* [2007] and *Hosseinpur et al.* [2009], Hall term effects are retained by relating the magnitude of b, as generated by Hall's term in equation (A3), to the compressible component of $\boldsymbol{U}_\perp$, absent in our incompressible model. By Helmholtz decomposition, this should enter through an irrotational contribution, $\boldsymbol{U}_\perp = \nabla\varphi\times\boldsymbol{e}_z + \nabla\chi$, related to the scalar field χ; in turn, the components u_z^e and U_z should also be retained. This immediately highlights the most delicate point concerning the $\boldsymbol{J}\times\boldsymbol{B}$ term in Ohm's law, already pointed out at the end of the previous section: due to the direct relation between b and χ, the (in)compressibility assumption plays a major role in determining the extent of Hall physics retained in the model. Remarkably, if $\partial_z = 0$, the in-plane incompressibility $\nabla\cdot\boldsymbol{U}_\perp = 0$ is admitted both in the $\boldsymbol{E}\times\boldsymbol{B}$ drift regime of the low-β limit, where b is neglected with respect to the strong guide field, and in the high-β limit, where the large kinetic (electron) pressure implies the smallness of both $\nabla\cdot\boldsymbol{U} = 0$ and $\nabla\cdot\boldsymbol{u}^e = 0$.

Acknowledgments
The authors are grateful to Francesco Pegoraro for discussions and comments. D.D.S. is in debt with Maurizio Ottaviani for many interesting discussions and, in particular, for having pointed out the possible importance of the ideal tearing during the nonlinear stage of primary reconnection instabilities and with Alessandro Biancalani for discussions about the explosive reconnection regime and for having kindly provided details about the numerical simulations performed in *Biancalani and Scott* [2011, 2012]. We thank W.H. Matthaeus and other two anonymous reviewers for useful comments. This research was partially supported by the joint training PhD program in Astronomy, Astrophysics, and Space Science between the University of Rome "Tor Vergata" and "Sapienza." No data were used in producing this manuscript other than those mentioned and available in the references. The data in the figures were generated by solving the (linear) differential equations in the paper with the given boundary conditions; the information required to reproduce them is therefore contained within the paper.

References

Ali, A., J. Li, and Y. Kishioto (2014), On the abrupt growth dynamics of nonlinear resistive tearing mode and the viscosity effects, *Phys. Plasmas*, *21*(5), 05312.

Angelopoulos, V., A. Runov, X.-Z. Zhou, D. L. Turner, S. A. Kiehas, S.-S. Li, and I. Shinohara (2014), Electromagnetic energy conversion at reconnection fronts, *Science*, *341*(5), 1478–1482.

Ara, G., B. Basu, B. Coppi, G. Laval, M. N. Rosenbluth, and B. V. Waddell (1978), Magnetic reconnection and $m = 1$ oscillations in current carrying plasmas, *Ann. Phys.*, *112*(2), 443–476.

Attico, N., F. Califano, and F. Pegoraro (2000), Fast collisionless reconnection in the whistler frequency range, *Phys. Plasmas*, *7*(6), 2381–2387.

Avinash, K., S. V. Bulanov, T. Eisrkepov, P. Kaw, F. Pegoraro, P. V. Sasarov, and A. Sen (1998), Forced magnetic field line reconnection in electron magnetohydrodynamics, *Phys. Plasmas*, *5*(8), 2849.

Battacharjee, A., Y.-M. Huang, H. Yang, and B. N. Rogers (2009), Fast reconnection in high-Lundquist-number plasmas due to the plasmoid instability, *Phys. Plasmas*, *16*(11), 112102.

Bian, N. H., and G. Vekstein (2007), Is the "out-of-plane" magnetic perturbation always a quadrupole in the Hall-mediated magnetic reconnection?, *Phys. Plasmas*, *14*(12), 120702.

Biancalani, A., and B. Scott (2011), Nonlinear growth acceleration in gyrofluid simulations of collisionless reconnection, in *38th European Physical Society Conference on Plasma Physics, Strasbourg, France, 27 Jun.–1 Jul.*, vol. 35, edited by A. Becoulet, T. Hoang, and U. Stroth, Eur. Phys. Soc., Geneva, Switzerland.
Biancalani, A., and B. Scott (2012), Observation of explosive collisionless reconnection in 3D nonlinear gyrofluid simulations, *Euro Phys. Lett.*, *97*(1), 15005.
Birn, J., et al. (2001), Geospace Environmental Modeling (GEM) magnetic reconnection challenge, *J. Geophys. Res.*, *106*(A3), 3715–3719.
Biskamp, D. (1986), Magnetic reconnection via current sheets, *Phys. Fluids*, *29*(5), 1520–1531.
Biskamp, D., E. Schwarz, and J. F. Drake (1995), Ion controlled collisionless magnetic reconnection, *Phys. Plasmas*, *75*(21), 3850.
Boozer, A. H. (2012), Magnetic reconnection in space, *Phys. Plasmas*, *19*(9), 092902.
Brackbill, J. U. (2011), A comparison of fluid and kinetic models of steady magnetic reconnection, *Phys. Plasmas*, *18*(3), 032309.
Brittnacher, M., K. B. Quest, and H. Karimabadi (1994), On the energy principle and ion tearing in the magnetotail, *Geophys. Res. Lett.*, *21*(15), 1591–1594.
Bulanov, S. V., F. Pegoraro, and A. S. Sakharov (1992), Magnetic recoonection in electron magnetohydrodynamics, *Phys. Fluids B*, *4*(8), 2499–2508.
Cai, H.-J., and L. C. Lee (1997), The generalized Ohm's law in collisionless magnetic reconnection, *Phys. Plasmas*, *4*(3), 509–520.
Cassak, P. A., R. N. Taylor, R. L. Fermo, M. T. Beidler, M. A. Shay, M. Swidsak, J. F. Drake, and H. Karimabadi (2015), Fast magnetic reconnection due to anisotropic electron pressure, *Phys. Plasmas*, *22*(2), 020705.
Comisso, L., D. Grasso, E. Tassi, and F. L. Waelbroeck (2012), Numerical investigation of a compressible gyrofluid model for collisionless reconnection, *Phys. Plasmas*, *19*(4), 042103.
Comisso, L., D. Grasso, F. L. Waelbroeck, and D. Borgogno (2013), Gyro-induced acceleration of magnetic reconnection, *Phys. Plasmas*, *20*(9), 092118.
Coppi, B. (1964a), "Inertial" instabilities in plasmas, *Phys. Lett.*, *11*(3), 226–228.
Coppi, B. (1964b), Addendum on inertial interchange modes, *Phys. Lett.*, *12*(3), 213–214.
Coppi, B. (1977), Topology of ballooning modes, *Phys. Rev. Lett.*, *39*(15), 939–942.
Coppi, B., G. Laval, and R. Pellat (1966), Dynamics of the geomagnetic tail, *Phys. Rev. Lett.*, *16*(26), 1207–1210.
Coroniti, F. V. (1985), Space plasma turbulent dissipation: Reality or myth?, *Space Sci. Rev.*, *42*(3–4), 399–410.
Daughton, W. (1999), The unstable eigenmodes of a neutral sheet, *Phys. Plasmas*, *6*(4), 1329–1343.
Daughton, W., and H. Karimabadi (2005), Kinetic theory of collisionless tearing at the magnetopause, *J. Geophys. Res.*, *110*, A03217, doi:10.1029/2004JA010751.
Daughton, W., V. Roytershteyn, H. Karimabadi, L. Yin, B. J. Albright, B. Bergen, and K. J. Bowers (2011), Role of electron physics in the development of turbulent magnetic reconnection in collisionless plasmas, *Nat. Phys.*, *7*, 539–542.
Del Sarto, D., F. Califano, and F. Pegoraro (2003), Secondary instabilities and vortex formation in collisionless-fluid magnetic reconnection, *Phys. Rev. Lett.*, *91*(23), 235001.
Del Sarto, D., F. Califano, and F. Pegoraro (2005), Current layer cascade in electron-magnetohydrodynamic reconnection and electron compressibility effects, *Phys. Plasmas*, *12*(1), 012317.
Del Sarto, D., F. Califano, and F. Pegoraro (2006), Electron parallel compressibility in the nonlinear development of two-dimensional magnetohydrodynamic reconnection, *Mod. Phys. Lett. B*, *20*(16), 931–961.
Del Sarto, D., C. Marchetto, F. Pegoraro, and F. Califano (2011), Finite Larmor radius effects in the nonlinear dynamics of collisionless magnetic reconnection, *Plasma Phys. Controlled Fusion*, *53*(3), 035008.
Del Sarto, D., F. Pegoraro, and F. Califano (2015), Pressure anisotropy and small spatial scales induced by velocity shear, ArXiv:1507.04895.
Drake, J. F., and Y. C. Lee (1977), Kinetic theory of tearing instabilities, *Phys. Fluids*, *20*(8), 035008.
Eastwood, J. P., T. D. Phan, S. D. Bale, and A. Tjulin (2009), Observation of turbulence generated by magnetic reconnection, *Phys. Rev. Lett.*, *102*(3), 035001.
Fruchtman, A., and Y. Maron (1991), Fast magnetic-field penetration into plasma due to the Hall field, *Phys. Fluids B*, *3*(7), 1546.
Fruchtman, A., and H. R. Strauss (1993), Modification of short scale-length tearing modes by the Hall field, *Phys. Fluids B*, *5*(5), 1408–1412.
Furth, H. P., J. Killeen, and M. N. Rosenbluth (1963), Finite-resistivity instabilities of a sheet pinch, *Phys. Fluids*, *6*(4), 459–484.
Galeev, A. A., and L. M. Zelenyi (1976), Tearing instability in plasma configurations, *J. Exp. Theor. Phys.*, *70*(6), 2133–2151.
Grasso, D., F. Pegoraro, F. Porcelli, and F. Califano (1999), Hamiltonian magnetic reconnection, *Plasma Phys. Controlled Fusion*, *41*, 1497–1515.
Grasso, D., E. Tassi, and F. L. Waelbroeck (2010), Nonlinear gyrofluid simulations of collisionless reconnection, *Phys. Plasmas*, *17*(8), 082312.
Hewett, D. W., G. E. Frances, and C. E. Max (1988), New regimes of magnetic reconnection in collisionless plasmas, *Phys. Rev. Lett.*, *61*(7), 893.
Hosseinpur, M., N. Bian, and G. Vekstein (2009), Two-fluid regimes of the resistive and collisionless tearing instability, *Phys. Plasmas*, *16*(1), 012104.
Kimura, K., and P. J. Morrison (2014), On energy conservation in extended magnetohydrodynamics, *Phys. Plasmas*, *21*(8), 082101.
Kingsep, S., K. V. Chukbar, and V. V. Yan'kov (1990), Electron magnetohydrodynamics, in *Reviews of Plasma Physics*, vol. 16, edited by B. Kadomtsev, pp. 243–291, Consultant Bureau, New York.
Kivelson, M., and C. T. Russell (1995), *Introduction to Space Physics*, Cambridge Univ. Press, Cambridge, U. K.
Kleva, R. G., J. F. Drake, and F. L. Waelbroeck (1995), Fast reconnection in high temperature plasmas, *Phys. Plasmas*, *2*(1), 23.
Krall, N. A., and A. W. Trivelpiece (1973), *Princples of Plasma Physics*, McGraw-Hill, New York.
Kutznesova, M. M., and M. Hesse (1998), Kinetic quasi-viscous and bulk flow inertia effects in collisionless magnetotail reconnection, *J. Geophys. Res.*, *103*(A1), 199–213.
Jain, N., and A. S. Sharma (2015), Evolution of electron current sheets in collisionless magnetic reconnection, *Phys. Plasmas*, *22*(10), 102110.
Landi, S., L. Del Zanna, E. Papini, F. Pucci, and M. Velli (2015), Resistive magnetohydrodynamic simulations of the ideal tearing mode, *Astrophys J.*, *806*(1), 131.
Laval, G., R. Pellat, and M. Vuillemin (1966), Instabilités electromagnetiques des plasmas sans collisions, in *Plasma Physics and Controlled Nuclear Fusion*, vol. 1, p. 259.
Lembege, B., and R. Pellat (1982), Stability of a thick two-dimensional quasineutral sheet, *Phys. Fluids*, *25*, 1995.
Lentini, M., and V. Pereyra (1974), A variable order finite difference method for nonlinear multipoint boundary value problems, *Math. Comput.*, *28*(128), 981–1003.
Loureiro, N. F., S. C. Cowley, W. D. Dorland, M. G. Haines, and A. A. Schekochihin (2005), X-point collapse and saturation in the nonlinear tearing mode reconnection, *Phys. Rev. Lett.*, *95*(23), 235003.
Loureiro, N. F., A. A. Schekochihin, and S. C. Cowley (2007), Instability of current sheets and formation of plasmoid chains, *Phys. Plasmas*, *14*(10), 0703.
Mandt, M. E., R. E. Denton, and J. F. Drake (1994), Transition to whistler mediated magnetic reconnection, *Geophys. Res. Lett.*, *21*(1), 73–76.

Matthaeus, W. H., and S. L. Lamkin (1985), Rapid magnetic reconnection caused by finite amplitude fluctuations, *Phys. Fluids*, *28*(1), 303.
Moser, A. L., and P. M. Bellan (2012), Magnetic reconnection from a multiscale instability cascade, *Nature*, *482*(2), 379–381.
Øieroset, M., T. D. Phan, M. Fujimoto, R. P. Lin, and R. P. Lepping (2001), In situ detection of collisionless reconnection in Earth's magnetotail, *Nature*, *412*(6845), 414–417.
Ottaviani, M., and F. Porcelli (1993), Nonlinear collisionless magnetic reconnection, *Phys. Rev. Lett.*, *71*(23), 3802.
Ottaviani, M., and F. Porcelli (1995), Fast nonlinear magnetic reconnection, *Phys. Plasmas*, *2*(11), 4104–4117.
Pegoraro, F., and T. J. Schep (1986), Theory of resistive modes in the ballooning representation, *Plasma Phys. Controlled Fusion*, *28*(4), 647.
Pegoraro, F., F. Porcelli, and T. J. Schep (1989), Internal kink modes in the ion-kinetic regime, *Phys. Fluids B*, *1*(2), 364–374.
Pegoraro, F., D. Borgogno, F. Califano, D. Del Sarto, E. Echkina, D. Grasso, T. Liseikina, and F. Porcelli (2004), Developments in the theory of collisionless reconnection in magnetic configurations with a strong guide field, *Nonlinear Processes Geophys.*, *11*, 567–577.
Pellat, R., F. V. Coroniti, and P. L. Pritchett (1991), Does ion tearing exist?, *Geophys. Res. Lett.*, *18*(2), 143–146.
Porcelli, F. (1991), Collisionless $m = 1$ tearing mode, *Phys. Rev. Lett.*, *66*(4), 425.
Porcelli, F., D. Boucher, and M. N. Rosenbluth (1996), Model for the sawtooth period amplitude, *Plasma Phys. Controlled Fusion*, *38*(12), 2163.
Porcelli, F., D. Borgogno, F. Califano, D. Grasso, and F. Pegoraro (2004), Magnetic reconnection: Collisionless regimes, *Phys. Scr. T.*, *107*, 153–158.
Pritchett, P. L. (2015), Instability of current sheets with a localized accumulation of magnetic flux, *Phys. Plasmas*, *22*(6), 062102.
Pucci, F., and M. Velli (2014), Reconnection of quasi-singular current sheets: The "ideal" tearing mode, *Astrophys. J. Lett.*, *780*(2), L19.
Quest, K. B., H. Karimabadi, and W. Daughton (2010), Linear theory of anisotropy driven modes in a Harris neutral sheet, *Phys. Plasmas*, *17*(2), 022107.
Rappazzo, F. A., and E. N. Parker (2013), Current sheets formation in tangled coronal magnetic fields, *Astrophys. J. Lett.*, *773*(1), L2.
Rebut, P. H., R. J. Bickerton, and B. E. Keen (1985), *The Joint European Torus: Installation, first results and prospects*, vol. 25, 1011.
Rogers, B. N., R. E. Danton, J. F. Drake, and M. A. Shay (2001), Role of dispersive waves in collisionless magnetic reconnection, *Phys. Rev. Lett.*, *87*(19), 1954004.
Schep, T. J., F. Pegoraro, and B. N. Kuvshinov (1994), Generalized two fluid theory of nonlinear magnetic structures, *Phys. Plasmas*, *1*(9), 2843–2852.
Schindler, K. (1974), A theory of the substorm mechanism, *J. Geophys. Res.*, *79*, 2803–2810.
Sergeev, V., D. G. Mitchell, C. T. Russell, and D. J. Williams (1993), Current sheet measurements within a flapping plasma sheet, *J. Geophys. Res.*, *98*(A10), 17,345–17,365.
Servidio, S., F. Valentini, F. Califano, and P. Veltri (2012), Local kinetic effects in two-dimensional plasma turbulence, *Phys. Rev. Lett.*, *108*(4), 045001.
Shibata, K., and T. Magara (2011), Solar flares: Magnetohydrodynamic processes, *Living Rev. Sol. Phys.*, *8*, 6.
Shibata, K., and S. Tanuma (2001), Plasmoid-induced-reconnection and fractal reconnection, *Earth Planets Space*, *53*(2), 473–482.
Sitnov, M. I., and K. Schindler (2010), Tearing stability of a multiscale magnetotail current sheet, *Geophys. Res. Lett.*, *37*, L08102, doi:10.1029/2010GL042961.
Sitnov, M. I., A. S. Sharma, P. N. Guzdar, and P. H. Yoon (2002), Reconnection onset in the tail of Earth's magnetosphere, *J. Geophys. Res.*, *107*(A9), 1256, doi:10.1029/2001JA009148.
Somov, B. V., and I. Verneta (1988), Magnetic reconnection in high-temperature plasmas of solar flares: III. Stabilizing effect of the transverse magnetic filed in a non-neutral current sheet, *Sol. Phys.*, *117*, 89–95.
Tenerani, A., A. F. Rappazzo, M. Velli, and F. Pucci (2015a), The tearing instability of thin current sheets: The transition to fast reconnection in presence of viscosity, *Astrophys. J.*, *801*(2), 145.
Tenerani, A., M. Velli, A. F. Rappazzo, and F. Pucci (2015b), Magnetic reconnection: Recursive current sheet collapse triggered by "ideal" tearing, *Astrophys. J. Lett.*, *813*(2), L32.
Vaivads, A., Y. Khotyaintsev, M. André, A. Retinò, S. C. Buchert, B. N. Rogers, P. Décréau, G. Paschmann, and T. D. Phan (2014), Structure of the magnetic reconnection diffusion region from four-spacecraft observations, *Phys. Rev. Lett.*, *93*(10), 105001.
Velli, M., and A. W. Hood (1989), Resistive tearing in line-tied magnetic fields: Slab geometry, *Sol. Phys.*, *119*(1), 107–124.
Velli, M., A. W. Hood, and G. Einaudi (1986), Resistive ballooning modes in line-tied coronal fields—Arcades, *Sol. Phys.*, *106*(2), 353–364.
Velli, M., A. W. Hood, and G. Einaudi (1987), Resistive ballooning modes in line-tied coronal fields—Loops, *Sol. Phys.*, *109*(2), 351–354.
Velli, M., A. W. Hood, and G. Einaudi (1990), Ideal kink instabilities in line-tied coronal loops—Growth rates and geometrical properties, *Astrophys. J.*, *350*, 428–436.
Velli, M., F. Pucci, F. Rappazzo, and A. Tenerani (2015), Models of coronal heating, turbulence and fast reconnection, *Philos. Trans. R. Soc. A*, *373*(2042), 20140262.
Waelbroeck, F. L. (1993), Onset of the sawtooth crash, *Phys. Rev. Lett.*, *70*(21), 3259.
Waelbroeck, F. L., R. D. Hazeltine, and P. J. Morrison (2009), A Hamiltonian electromagnetic gyrofluid model, *Phys. Plasmas*, *16*(3), 032109.
Wan, M., W. H. Matthaeus, S. Servidio, and S. Oughton (2013), Generation of X-points and secondary islands in 2D magnetohydrodynamic turbulence, *Phys. Plasmas*, *20*(4), 042307.
Wesson, J. A. (1990), Sawtooth reconnection, *Nucl. Fusion*, *30*(12), 2545.
Yamada, M., J. Yoo, J. Jara-Almonte, H. Ji, R. M. Kulsrud, and C. E. Myers (2014), Conversion of magnetic energy in the magnetic reconnection layer of a laboratory plasma, *Nat. Commun.*, *5*, 4774.
Yin, L., and D. Winske (2003), Plasma pressure tensor effects on reconnection: Hybrid and Hall-magnetohydrodynamic simulations, *Phys. Plasmas*, *10*(5), 1595.
Yu, Q., S. Günter, and K. Lackner (2014), Formation of plasmoids during sawtooth crashes, *Nucl. Fusion*, *54*(7), 072005.
Zank, G. P., and W. H. Matthaeus (1992), The equations of reduced magnetohydrodynamics, *J. Plasma Phys.*, *48*(1), 85–100.
Zeleney, L., A. Artemyev, H. Malova, and V. Popov (2008), Marginal stability of thin current sheets in the earth magnetotail, *J. Atmos. Sol. Terr. Phys.*, *70*, 325–333.
Zeleney, L., and A. Artemyev (2013), Mechanisms of spontaneous reconnection: From magnetospheric to fusion plasmas, *Space Sci. Rev.*, *178*, 441–457.
Zweibel, E., and M. Yamada (2009), Magnetic reconnection in astrophysical and laboratory plasmas, *Annu. Rev. Astron. Astrophys.*, *47*, 291–332.